Network Theoretical Transient Analysis of Signal Transmission Over Evanescent Modes

Abbas S. Omar and Aladin H. Kamel

***Abstract*—A network theoretical transient analysis of waveguide transmission of modulated signals with carrier frequencies below cutoff is presented. Both matched and mismatched terminations are considered. It is clearly shown that recent publications reporting on signal transmission faster than c (light velocity in free space) are based on erroneous interpretations of the measured results. It is also shown that the information capacity of tunneling systems is extremely low, which makes their use as communication channels unfavorable. A number of numerical experiments has been carried out. The achieved results justify the presented analysis and give the proper interpretations to the *seemingly* faster-than-c transmission reported recently.**

***Index Terms*—Electromagnetic transient analysis, transfer functions, transient response, waveguides.**

I. Introduction

In RECENT years, some publications reported on *measurable* signal transmission faster than c, which can be used for communications (see, e.g., [1] and [2]). The transmission of a carrier signal modulated by a narrow-band Gaussian baseband pulse in a TEM line section and an undersized (below cutoff) waveguide section of the same length was measured. It was observed that the arrival of the pulse at the end of the waveguide section is earlier than that at the end of the TEM line section. As the pulse transmission in TEM lines takes place at c, it was concluded that the pulse transmission in undersized waveguides is faster than c. These results were justified by the fact that the signal group velocity in undersized waveguides exceeds c. Applications to communication channels based on these results were also proposed with the conclusion that information can be transmitted superluminally (faster than c).

Pulse propagation in dispersive channels (e.g., undersized waveguides) has been comprehensively treated in the open literature (e.g., [3]–[6]). Sommerfeld, as well as Brillouin [3] and Jackson [4], demonstrated that for any passive (initially energy-free) dispersive medium and pulse shape, no signal can propagate faster than c. Physical measurements of pulse propagation in dispersive channels, which may show that pulses can *appear* to travel faster than c, have been adequately explained (e.g., [5] and [6]). Superluminality has been shown to be principally a direct consequence of the dispersive reshaping of the pulse form. Motivated by the revival of such discussions a number of publications have considered recently this and related subjects again (e.g., [7]–[11]).

Manuscript received February 16, 2001; revised January 31, 2002.
A. S. Omar is with the University of Magdeburg, Magdeburg, Germany.
A. H. Kamel is with RITSEC, Cairo, Egypt.
Digital Object Identifier 10.1109/TAP.2003.809824

The analysis presented in this contribution is basically network theoretical. It is supplemental to the well-established ones in the open literature (e.g., [3]–[6]) which are basically of a mathematical nature. A correct interpretation of the measurements reported in [1] and [2] will be given. It is based on a technique which uniquely assigns a point on the output signal to any given point on the input signal. Transmission velocities can then be unambiguously defined which are clearly shown not to exceed c.

This contribution begins with an analysis of the transfer function (frequency domain) and the related impulse response (time domain) of a waveguide section with different terminations. Baseband pulses of different forms modulating a carrier signal with a frequency below the cutoff of the waveguide signal-carrying mode are then applied at the input. With properly switching off the input signal, the aforementioned technique for uniquely relating points on the input and output signals is introduced. Case studies are then considered which clearly show the incorrectness of the assertion of faster-than-c signal transmission.

II. Basic Formulation

Let us consider an empty waveguide section of length L, which supports a TE or TM signal-carrying mode of a cutoff wave number $k_c = \omega_c/c$. As the spectrum of most of the input signals to be considered is dominantly below ω_c, we will characterize the waveguide mode through its attenuation constant $\alpha(\omega)$ and wave reactance $X(\omega)$ [rather than the propagation constant $\beta(\omega)$ and the wave impedance $Z_w(\omega)$]. Only the TE case will be considered here. TM analysis is essentially similar. For a TE mode, $\alpha(\omega)$ and $X(\omega)$ are given by (see e.g., [12])

$$\alpha(\omega) = \frac{1}{c}\sqrt{\omega_c^2 - \omega^2} \tag{1-a}$$

$$X(\omega) = Z_0 \frac{\omega}{\sqrt{\omega_c^2 - \omega^2}} \tag{1-b}$$

where Z_0 is the free space intrinsic impedance. Fig. 1 shows an equivalent line section which is excited by a voltage source of internal impedance Z_S and terminated with a load impedance Z_L. An ideal voltage source with $Z_S = 0$ is in fact equivalent to short circuiting the waveguide at its left-hand side (LHS) and backing the short circuit with a surface magnetic current (a technique usually used to deal with aperture coupling problems, see, e.g., [13]). The dual case of terminating the LHS of the waveguide with a magnetic wall backed with a surface electric current is equivalent to exciting the equivalent line with an ideal current source. A matched source, on the other hand, should have $Z_S = jX(\omega)$. Two load terminations will be considered: The

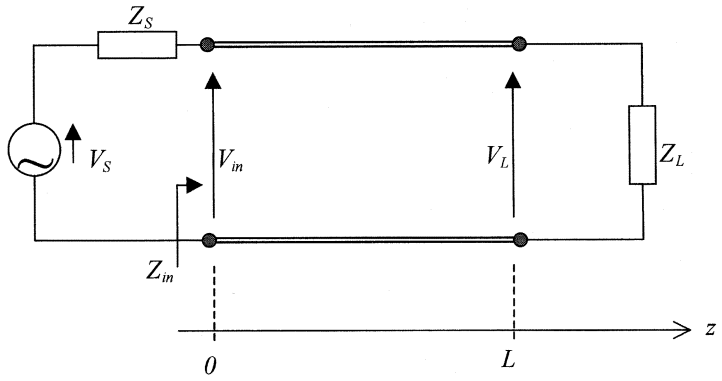

Fig. 1. Equivalent line section with source and load terminations.

matched load with $Z_L = jX(\omega)$ and a frequency independent load with $Z_L = Z_0$. For each of these loads, three types of exciting sources will be considered; an ideal voltage source, a matched source, and a source with a frequency independent internal impedance $Z_S = Z_0$. In the following cases, both the frequency-dependent transfer function $H(\omega)$ and its time-dependent inverse Fourier transform; the impulse response $h(t)$ will be revisited. They are given by

$$H(\omega) = \frac{V_L(\omega)}{V_S(\omega)} \tag{2-a}$$

$$h(t) = \frac{1}{2\pi}\int_{-\infty}^{+\infty} H(\omega)e^{j\omega t}\,d\omega \tag{2-b}$$

where $V_S(\omega)$ and $V_L(\omega)$ are the Fourier transforms of the source voltage $v_S(t)$ and the load voltage $v_L(t)$, respectively.

A. Matched Load Termination

For $Z_L = jX(\omega)$ no reflection takes place at the load side. The input impedance at $z = 0$ is independent of the line length and is equal to $jX(\omega)$ as well. The corresponding input voltage is equal to the source voltage (half of it) in case of ideal (matched) voltage source.

1) Ideal voltage source

$$Z_{in} = jX(\omega), \qquad V_{in} = V_S \tag{3-a}$$

$$H_1(\omega) = \frac{V_L(\omega)}{V_S(\omega)} = H_0(L, \omega) \tag{3-b}$$

where

$$H_0(z, \omega) = e^{-\alpha(\omega)\cdot z}. \tag{4}$$

2) Matched voltage source

$$V_{in} = \frac{V_S}{2} \tag{5-a}$$

$$H_2(\omega) = \frac{H_0(L, \omega)}{2}. \tag{5-b}$$

3) Source with $Z_S = Z_0$

$$V_{in} = V_S \cdot \frac{jX(\omega)}{Z_0 + jX(\omega)} \tag{6-a}$$

$$H_3(\omega) = \frac{H_0(L, \omega) - R_0(L, \omega)}{2} \tag{6-b}$$

where

$$R_n(z, \omega) = \left[\frac{\sqrt{\omega_c^2 - \omega^2} - j\omega}{\sqrt{\omega_c^2 - \omega^2} + j\omega}\right]^{(n+1)} \cdot e^{-\alpha(\omega)\cdot z} \qquad n = 0, 1, 2, 3, \ldots. \tag{7}$$

The impulse responses $h_1(t)$, $h_2(t)$, and $h_3(t)$ are given by

$$h_1(t) = h_0(L, t), \quad h_2(t) = \frac{h_0(L, t)}{2}$$

$$h_3(t) = \frac{h_0(L, t) - r_0(L, t)}{2} \tag{8}$$

where

$$h_0(z, t) = \frac{1}{2\pi}\int_{-\infty}^{\infty} e^{(j\omega t - \alpha(\omega)\cdot z)}\,d\omega \tag{9-a}$$

$$r_n(z, t) = \frac{1}{2\pi}\int_{-\infty}^{\infty}\left[\frac{\sqrt{\omega_c^2 - \omega^2} - j\omega}{\sqrt{\omega_c^2 - \omega^2} + j\omega}\right]^{(n+1)} \cdot e^{(j\omega t - \alpha(\omega)\cdot z)}\,d\omega, \qquad n = 0, 1, 2, 3, \ldots. \tag{9-b}$$

B. Frequency Independent Load Impedance $Z_L = Z_0$

Due to the fact that $Z_0 \neq jX$, reflection at the load side must take place. The matching condition at the generator side will determine whether this reflection is a single or a multiple one.

1) Ideal voltage source

$$H_4(\omega) = \frac{H_0(L, \omega) + R_0(L, \omega)}{1 + R_0(2\cdot L, \omega)}. \tag{10-a}$$

The transfer function $H_4(\omega)$ can be rewritten as a geometrical series

$$H_4(\omega) = [H_0(L, \omega) + R_0(L, \omega)]\cdot[1 - R_0(2\cdot L, \omega) + R_1(4\cdot L, \omega) - R_2(6\cdot L, \omega) + \cdots]. \tag{10-b}$$

The earlier geometrical-series expansion resembles the multiple refection between the load and generator sides of the line section. The term $R_n(2\cdot(n+1)\cdot L, \omega)$ in the RHS brackets of (10-b) accounts for the $n + 2^{nd}$ load-side reflection, while the alternating sign of R_n accounts for the short-circuit reflection at the generator side due to the zero internal impedance of the ideal voltage source.

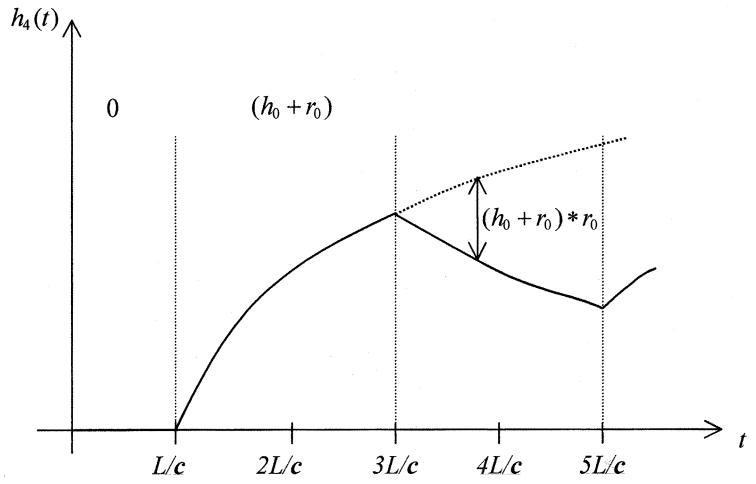

Fig. 2. Schematic diagram of $h_4(t)$.

2) Matched voltage source

$$H_5(\omega) = \frac{H_0(L, \omega) + R_0(L, \omega)}{2}. \tag{11}$$

The transfer function $H_5(\omega)$ is half the contribution of the first load-reflection in $H_4(\omega)$ [compare with the relation between $H_1(\omega)$ and $H_2(\omega)$].

3) Source with $Z_S = Z_0$

$$H_6(\omega) = \frac{H_0(L, \omega) - R_1(L, \omega)}{2 \cdot [1 - R_1(2 \cdot L, \omega)]}. \tag{12-a}$$

Again, $H_6(\omega)$ can be rewritten as a geometrical series in order to resemble its multiple reflection nature

$$H_6(\omega) = \frac{H_0(L, \omega) - R_1(L, \omega)}{2} \cdot [1 + R_1(2 \cdot L, \omega) + R_3(4 \cdot L, \omega) + R_5(6 \cdot L, \omega) + \cdots]. \tag{12-b}$$

Each term in the earlier geometrical series represents a pair of reflections; once at the generator side and once at the load side of the line section.

The impulse responses $h_4(t)$, $h_5(t)$, and $h_6(t)$ can be obtained by making use of the product $\leftrightarrow$ convolution property of the Fourier transform

$$h_4(t) = [h_0(L, t) + r_0(L, t)] * [\delta(t) - r_0(2 \cdot L, t) + r_1(4 \cdot L, t) - r_2(6 \cdot L, t) + \cdots] \tag{13-a}$$

$$h_5(t) = \frac{h_0(L,t) + r_0(L,t)}{2} \tag{13-b}$$

$$h_6(t) = \frac{h_0(L,t) - r_1(L,t)}{2} * [\delta(t) + r_1(2 \cdot L, t) + r_3(4 \cdot L, t) + r_5(6 \cdot L, t) + \cdots]. \tag{13-c}$$

As will be shown shortly, $h_0(z, t)$ as well as all $r_n(z, t)$ vanish identically for $t < (z/c)$. In addition, it is readily shown that the convolution of two functions $f_1(t)$ and $f_2(t)$ (which identically vanish for $t < t_1$ and $t < t_2$, respectively) vanishes identically for $t < (t_1 + t_2)$. The effect of the multiple reflection in (13-a) and (13-c) will then appear successively for $t \geq (L/c)$, $t \geq (3 \cdot L/c)$, $t \geq (5 \cdot L/c)$, ... etc., as shown in (14-a) and (14-b) at the bottom of the next page.

The successive appearance feature related to the multiple reflection is schematically shown in Fig. 2 for $h_4(t)$. Each time a reflection at the load side of the line section takes place (i.e., at $t = (L/c)$, $t = (3 \cdot L/c)$, $t = (5 \cdot Lc)$, ... etc.), a corresponding contribution changes the impulse response.

Based on the earlier discussion, it is easily seen that for a source voltage $v_S(t)$ with a first appearance at $t = 0$ [i.e., $v_S(t) = 0$ for $t < 0$] the first appearance of the load voltage $v_L(t)$ [which is given by the convolution $v_L(t) = h(t) * v_S(t)$] occurs not earlier than $t = (L/c)$. This is due to the fact that all $h(t)$ considered earlier vanish identically for $t < (L/c)$ and hence $v_L(t) = 0$ for $t < (L/c)$. The propagation of (at least) the first appearance of the signal cannot then be faster than c (as it must be).

C. Calculation of $h_0(z, t)$ and $r_n(z, t)$

Let us consider the generating function $g(z, t)$ and its Fourier transform $G(z, \omega)$ which are given by

$$G(z, \omega) = \frac{e^{-\alpha(\omega) \cdot z}}{c \cdot \alpha(\omega)} = \frac{e^{-(z/c) \cdot \sqrt{\omega_c^2 - \omega^2}}}{\sqrt{\omega_c^2 - \omega^2}} \tag{15-a}$$

$$g(z, t) = \frac{1}{2\pi} \int_{-\infty}^{\infty} \frac{e^{(j\omega t - (z/c) \cdot \sqrt{\omega_c^2 - \omega^2})}}{\sqrt{\omega_c^2 - \omega^2}} \, d\omega. \tag{15-b}$$

The inverse Fourier transform in (15-b) has the following closed-form expression [14]

$$g(z, t) = u\left(t - \frac{z}{c}\right) \cdot J_0\left(\omega_c \cdot \sqrt{t^2 - \left(\frac{z}{c}\right)^2}\right) \tag{15-c}$$

where $u(x)$ and $J_n(x)$ are the unit step function and the n^{th} order ordinary Bessel function, respectively. It is readily shown that $h_0(z, t)$ and $r_0(z, t)$ are related to $g(z, t)$ according to

$$h_0(z, t) = -c \cdot \frac{\partial}{\partial z} g(z, t) \tag{16-a}$$

$$r_0(z, t) = \frac{2c}{\omega_c^2} \cdot \frac{\partial}{\partial z}\left(\frac{\partial h_0}{\partial t} + c \cdot \frac{\partial h_0}{\partial z}\right) - h_0(z, t). \tag{16-b}$$

Detailed analysis and complete expressions for $r_n(z, t)$ for

arbitrary n are given in [15]. Explicit expressions for $h_0(z, t)$ and $r_0(z, t)$ are easily shown to be given by (17-a) and (17-b) as shown at the bottom of the page.

III. Results and Discussions

Let us first express the load voltage $v_L(t)$ (output signal) in terms of the source voltage $v_S(t)$ (input signal) which will be assumed vanishing identically for $t < 0$ (i.e., being switched-on at $t = 0$). Due to the fact that $v_S(t) = 0$ for $t < 0$ and $h(t) = 0$ for $t < (L/\boldsymbol{c})$, the convolution integral describing $v_L(t)$ is reduced to

$$v_L(t) = \int_{(L/c)}^{t} h(t') \cdot v_S(t - t')\, dt'. \tag{18-a}$$

In order to deal with normalized quantities, time and delay angles ($\theta = \omega_o \cdot t$) and ($\theta_o = \omega_o \cdot L/\boldsymbol{c}$) are introduced, respectively, where ω_o is an arbitrary normalizing frequency. The earlier equation can then be rewritten as

$$v_L(\theta) = \int_{\theta_0}^{\theta} h(\theta') \cdot v_S(\theta - \theta')\, d\theta' \tag{18-b}$$

where $h(\theta) = h(t)/\omega_0$. Fig. 3 shows $(h_0(\theta_0, \theta) - \delta(\theta - \theta_0))$ [which corresponds to the second term in the RHS of (17-a)] and $r_0(\theta_0, \theta)$, as being the frequently appearing functions in the different impulse responses derived earlier, for $\theta_o = 5 \cdot \pi$ and different values of (ω_c/ω_0). For $\omega_c \gg \omega_0$ [Fig. 3(a)], $(h_0(\theta_0, \theta) - \delta(\theta - \theta_0))$ resembles the behavior of a negative Dirac-delta at $\theta = \theta_0$ [Fig. 3(a)-(c)] in addition to a highly oscillating term [zoomed in Fig. 3(b)] which represents in fact $h_0(\theta_0, \theta)$. The function $r_0(\theta_0, \theta)$ [Fig. 3(c)] resembles the same high oscillation behavior as $h_0(\theta_0, \theta)$. For input signals with a spectrum around or below ω_0, the high oscillation of $h_0(\theta_0, \theta)$ and $r_0(\theta_0, \theta)$ will be averaged out to zero in (18-b) rendering a negligibly small output signal. This confirms the fact that for $\omega_c \gg \omega_0$ no appreciable signal transmission can take place. On the other hand, for $\omega_c \ll \omega_0$ [Fig. 3(d)–(e)] both $(h_0(\theta_0, \theta) - \delta(\theta - \theta_0))$ and $r_0(\theta_0, \theta)$ are negligibly small, which confirms the nearly TEM transmission of signals with a spectrum around or above ω_0. For $\omega_c \approx \omega_0$ [Fig. 3(f)–(g)] $h_0(\theta_0, \theta)$ and $r_0(\theta_0, \theta)$ have the same oscillation behavior as input signals with a spectrum around ω_0. High interaction between $h(\theta')$ and $v_S(\theta - \theta')$ in (18-b) should be expected,

$$h_4(t) = \begin{cases} 0 & \cdots & t < (L/c) \\ [h_0(L, t) + r_0(L, t)] & \cdots & (L/c) \le t < (3 \cdot L/c) \\ [h_0(L, t) + r_0(L, t)] * [\delta(t) - r_0(2 \cdot L, t)] & \cdots & (3 \cdot L/c) \le t < (5 \cdot L/c) \\ [h_0(L, t) + r_0(L, t)] * [\delta(t) - r_0(2 \cdot L, t) + r_1(4 \cdot L, t)] & \cdots & (5 \cdot L/c) \le t < (7 \cdot L/c) \\ \cdots & \cdots & \cdots \\ \cdots & \cdots & \cdots \\ \cdots & \cdots & \cdots \end{cases} \tag{14-a}$$

$$h_6(t) = \frac{1}{2} \cdot \begin{cases} 0 & \cdots & t < (L/c) \\ [h_0(L, t) - r_1(L, t)] & \cdots & (L/c) \le t < (3 \cdot L/c) \\ [h_0(L, t) - r_1(L, t)] * [\delta(t) + r_1(2 \cdot L, t)] & \cdots & (3 \cdot L/c) \le t < (5 \cdot L/c) \\ [h_0(L, t) - r_1(L, t)] * [\delta(t) + r_1(2 \cdot L, t) + r_3(4 \cdot L, t)] & \cdots & (5 \cdot L/c) \le t < (7 \cdot L/c). \\ \cdots & \cdots & \cdots \\ \cdots & \cdots & \cdots \\ \cdots & \cdots & \cdots \end{cases} \tag{14-b}$$

$$h_0(z, t) = \delta\left(t - \frac{z}{c}\right) - u\left(t - \frac{z}{c}\right) \cdot \frac{\omega_c \cdot \frac{z}{c} \cdot J_1\left(\omega_c \cdot \sqrt{t^2 - \left(\frac{z}{c}\right)^2}\right)}{\sqrt{t^2 - \left(\frac{z}{c}\right)^2}} \tag{17-a}$$

$$r_0(z, t) = \frac{u\left(t - \frac{z}{c}\right)}{(t + \frac{z}{c})^2} \cdot \left\{ \begin{array}{c} 2 \cdot \left(t - \frac{z}{c}\right) \cdot \left[2 \cdot \frac{J_1\left(\omega_c \cdot \sqrt{t^2 - \left(\frac{z}{c}\right)^2}\right)}{\omega_c \cdot \sqrt{t^2 - \left(\frac{z}{c}\right)^2}} - J_0\left(\omega_c \cdot \sqrt{t^2 - \left(\frac{z}{c}\right)^2}\right) \right] \\ + \omega_c \cdot \sqrt{t^2 - \left(\frac{z}{c}\right)^2} \cdot \frac{z}{c} \cdot J_1\left(\omega_c \cdot \sqrt{t^2 - \left(\frac{z}{c}\right)^2}\right) \end{array} \right\} \tag{17-b}$$

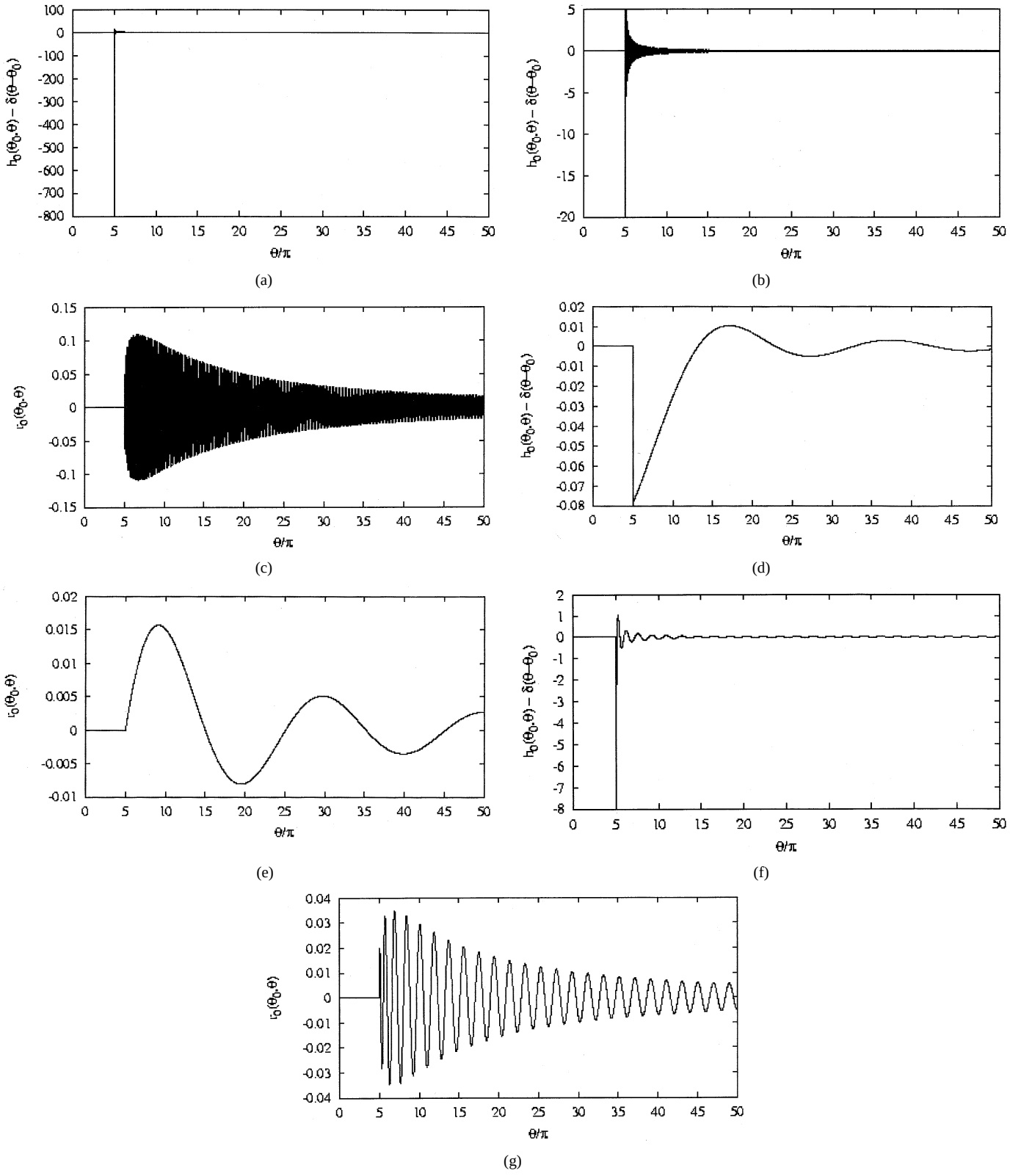

Fig. 3. Impulse responses $(h_0(\theta_0,\ \theta) - \delta(\theta_0 - \theta))$ and $r_0(\theta_0,\ \theta)$ for $\omega_c = 10 \cdot \omega_0$ (a)–(c), $\omega_c = 0.1 \cdot \omega_0$ (d) and (e) and $\omega_c = \omega_0$ (f) and (g).

which accounts for the fact that mismatching and the related reflection effects are appreciable in this frequency range.

Next, the contribution of the input signal v_S to the load signal v_L as being given by (18-b) is schematically shown in Fig. 4 by the dashed area. As is easily seen, the output signal $v_L(\theta)$ at a given θ contains information about the input signal $v_S(\varphi)$ within the range $0 \leq \quad \varphi < (\theta - \theta_0)$ only. The first *appearance* or *arrival* of $v_S(\theta)$ at the output cannot then be detected earlier than $(\theta + \theta_0)$, and is hence not faster than $\boldsymbol{c}$. If a peak would appear in $v_L(\theta)$ at $\theta < (\theta_m + \theta_0)$ it must be an integration effect of the leading part of v_S [due to the convolution integral in (18-b)] and not at all due to its maximum at θ_m.

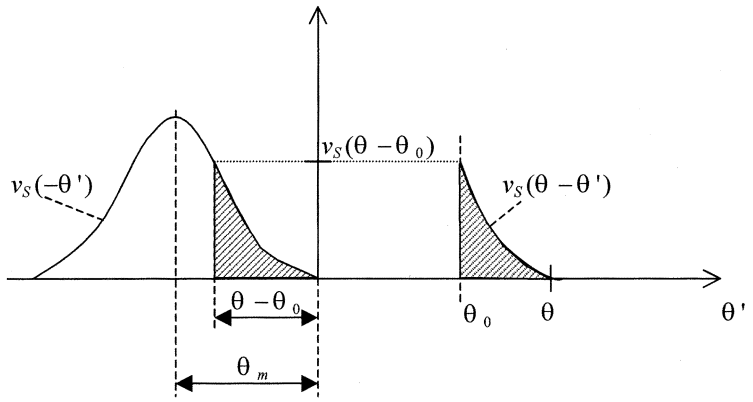

Fig. 4. Schematic diagram of the convolution integral in (18-b).

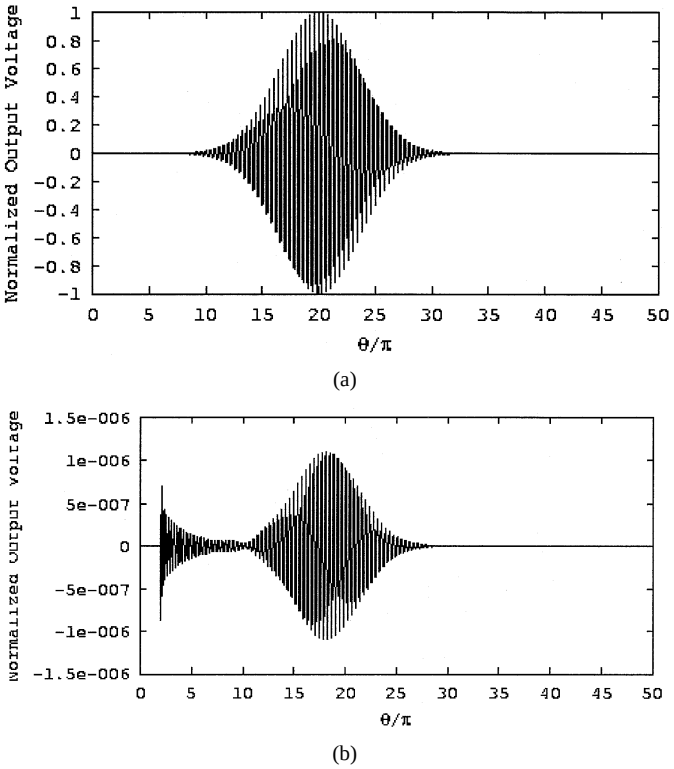

Fig. 5. TEM output (a) and waveguide output (b) signals of case 1. Input signal is a carrier of $\omega_{\text{carrier}} = 0.91 \cdot \omega_{\text{cutoff}}$ modulated by a Gaussian pulse with $\theta_\tau = 5 \cdot \pi$ and $\theta_m = 18 \cdot \pi$, which is not switched-off.

In order to give the correct explanation to the wrongly interpreted faster-than-c signal transmission reported in, e.g., [1] and [2], the output signals at the end of a TEM line and that of a waveguide section of the same length (both excited by the same input signal) have been calculated. The delay angle of both the TEM line and the waveguide has been fixed to $\theta_o = 2 \cdot \pi$. The input signal is a carrier modulated by a baseband pulse(s) of different forms, which is switched at $\theta = 0$. The input signal in all cases considered below is not shown. Instead the output of the TEM line (which is identical to the input signal shifted by θ_o) is plotted.

In the following four cases, the carrier frequency has been fixed to five times $\omega_o (\omega_{\text{carrier}} = 5 \cdot \omega_o)$, while the cutoff frequency of the waveguide section (will be denoted by ω_{cutoff} instead of ω_c) has been chosen higher than $\omega_{\text{carrier}} (\omega_{\text{cutoff}} = 5.5 \cdot \omega_o)$. The baseband signal is a Gaussian pulse of ($\theta_\tau = \omega_0 \cdot \tau = 5 \cdot \pi$). Its maximum is located at $\theta_m = 3.6 \cdot \theta_\tau$ in cases 1 and 2 and at $\theta_m = 4 \cdot \theta_\tau$ in cases 3 and 4. For all four cases, $v_s(\theta)$ is then given by

$$v_S(\theta) = u(\theta) \cdot e^{-((\theta - \theta_m)/\theta_\tau)^2} \cdot \cos\left(\frac{\omega_{\text{carrier}}}{\omega_0} \cdot \theta\right). \quad (19)$$

Cases 1 and 2: In case 1, the input signal is let to approach zero as $t \to \infty$ (no switch-off). Although the switching-on is not detected in the TEM output [Fig. 5(a)], it is clearly detected in the waveguide output [Fig. 5(b)]. The reason is the high-pass effect of the evanescent waveguide, which strengthens the higher frequency components included in the switch-on process as compared to the lower frequency ones. The total detectable extension of the waveguide output signal is about $26 \cdot \pi$ (from $2 \cdot \pi$ to about $28 \cdot \pi$). The waveguide output resembles a peak and the question, whether this peak corresponds to the maximum of the TEM output, remains open.

In order to answer the earlier question, the input signal has been switched-off at its maximum in case 2. Fig. 6(a) represents the corresponding TEM output. Due to the sudden switch-off, most of the input-signal spectrum lies above cutoff. The waveguide output [Fig. 6(c)]) is many orders of magnitudes higher than that of the previous case. It looks as if it exists after the switch-off of the input signal only. In Fig. 6(b) the waveguide output has been zoomed with the same resolution as in the previous case. Now we can recognize that the first portion of waveguide output (from $2 \cdot \pi$ to $20 \cdot \pi$) is identical to the corresponding portion in the previous case. It jumps at $\theta = 20 \cdot \pi$ (exactly the switch-off point of the TEM output) to the higher energy level. It is easily seen now that the maximum of the input pulse (which is now associated with the sudden switch-off) does not correspond to the peaks of the waveguide output.

We can conclude then that before speaking about propagation speeds, we have to first find a technique that uniquely assigns a point on the waveguide output to a given point on the input. The technique described earlier (just switch-off the input signal at a given point and look for the point on the waveguide output at which the energy level jumps) seems to fulfill our needs. In the case considered here (case 2), we can easily see that the points on the waveguide output corresponding to the beginning

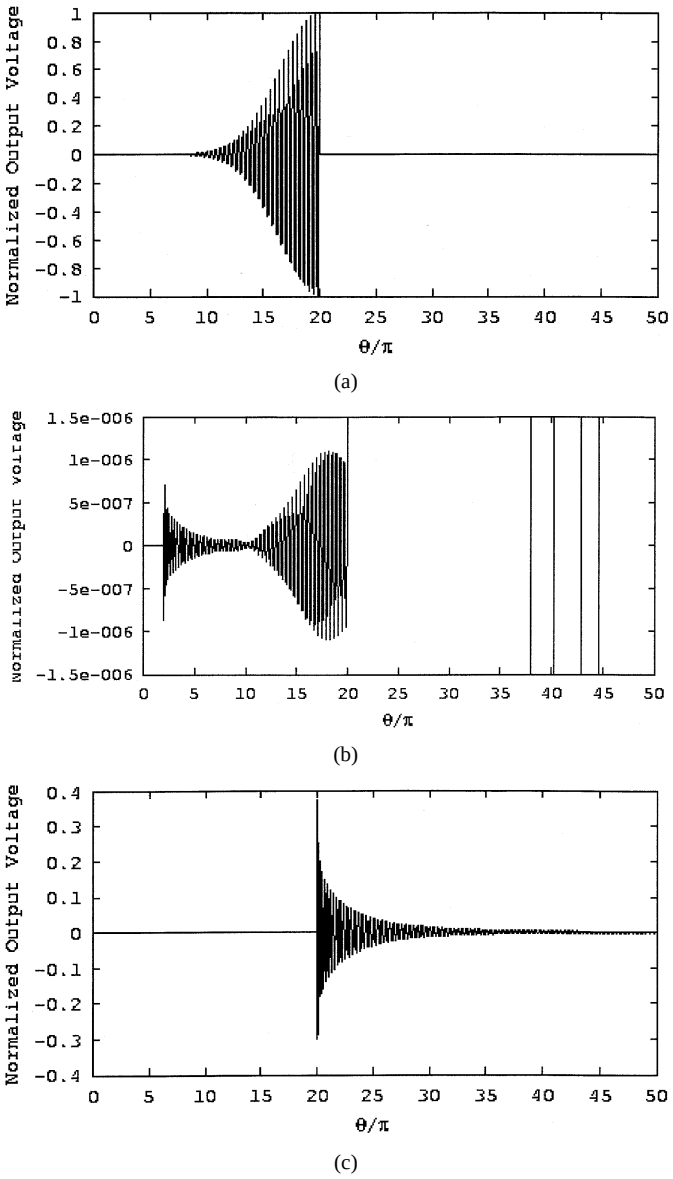

Fig. 6. TEM output (a) zoomed waveguide output (b), non-zoomed waveguide output signals of case 2. Input signal is a carrier of $\omega_{\text{carrier}} = 0.91 \cdot \omega_{\text{cutoff}}$ modulated by a Gaussian pulse with $\theta_\tau = 5 \cdot \pi$ and $\theta_m = 18 \cdot \pi$, which is switched off at its maximum.

(switch-on) and the end (switch-off) of the input signal propagate with exactly ***c***. The mistake made in [1], [2] is mainly due to associating the maximum of the input pulse with the peak of the waveguide output (as will be shown shortly). The fact that the waveguide outputs in Fig. 5(b) and Fig. 6(b) are identical in the range where the corresponding inputs are identical is a justification for obeying the causality, as the output signal in the aforementioned coincidence range ($\theta = 2 \cdot \pi$ to $\theta = 20 \cdot \pi$) has not been able to forecast the future of the input signal in the subsequent range ($\theta > 20 \cdot \pi$).

Cases 3 and 4: Here, the sudden switch-on of the input signal at $\theta = 0$ (which corresponds to $\theta = \theta_o$ in the TEM output) has been depressed by choosing $\theta_m = 4 \cdot \theta_\tau$. Again, two cases have been studied. In case 3, the input has not been switched-off. This together with the very weak switching-on lead to an input-signal spectrum well below cutoff, which explains the very low energy level (voltage level 10^{-6}) of the waveguide-output signal [Fig. 7(b)]. In case 4, the input pulse has been switched-off at its maximum. Again, due to the sudden switch-off, the input-signal spectrum contains predominantly frequency components well above cutoff and the waveguide-output-signal energy level is relatively high [Fig. 8(c)]. If we zoom it with the same resolution of the previous case [i.e., that of Fig. 7(b)], we get Fig. 8(b). Again, the first portion (from $\theta = 2 \cdot \pi$ to $\theta = 22 \cdot \pi$) of both Figs. 7(b) and 8(b) are identical and hence the waveguide output in the aforementioned range has not been able to forecast the input in the subsequent range. Starting from the switch-off point, the waveguide output [Fig. 8(c)] jumps from the lower energy level (voltage level 10^{-6}) to the higher energy level (voltage level 10^{-1}). This jumping point can be uniquely associated with the TEM-output maximum, or equivalently the maximum of the input pulse. It is clear then that the pulse maximum (according to our unique association rule) propagates at exactly ***c***. An association of the input-pulse maximum with the peak of the waveguide output would lead to the erroneous conclusion of propagation faster than ***c***.

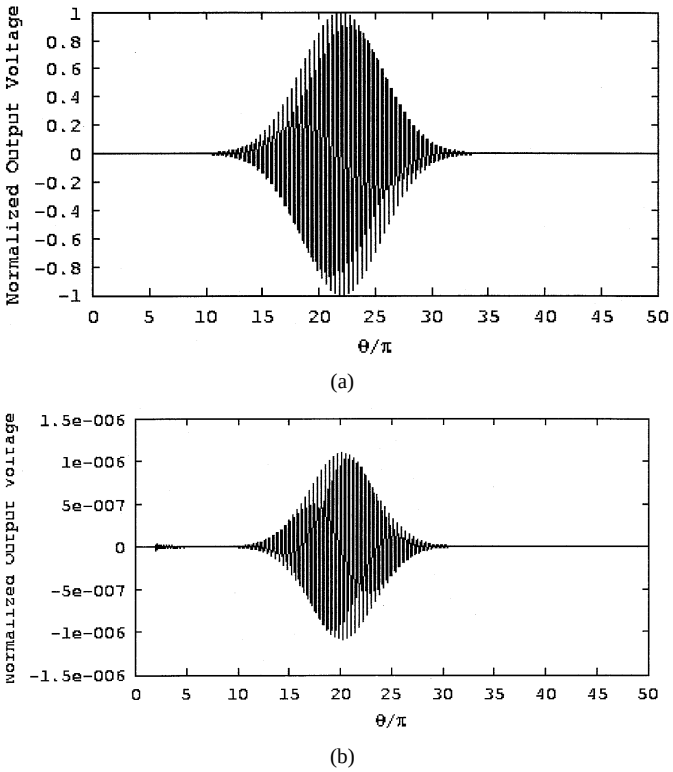

Fig. 7. TEM output (a), waveguide output (b), and waveguide output signals of case 3. Input signal is a carrier of $\omega_{\text{carrier}} = 0.91 \cdot \omega_{\text{cutoff}}$ modulated by a Gaussian pulse with $\theta_\tau = 5 \cdot \pi$ and $\theta_m = 20 \cdot \pi$, which is not switched off.

We can conclude now that the switch-off "trick" is an efficient mean for providing a unique association between points on input and output signals. Principally, this technique can be applied to points other than the maximum. For finding out the point on the waveguide output corresponding to a certain point on the input signal, we switch-off the input signal at this point. Due to the generation of higher frequency components which is associated with the sudden switch-off, the output jumps at this point from a lower to a higher energy level. Due to the causality, the output cannot forecast this witch-off before it takes place and

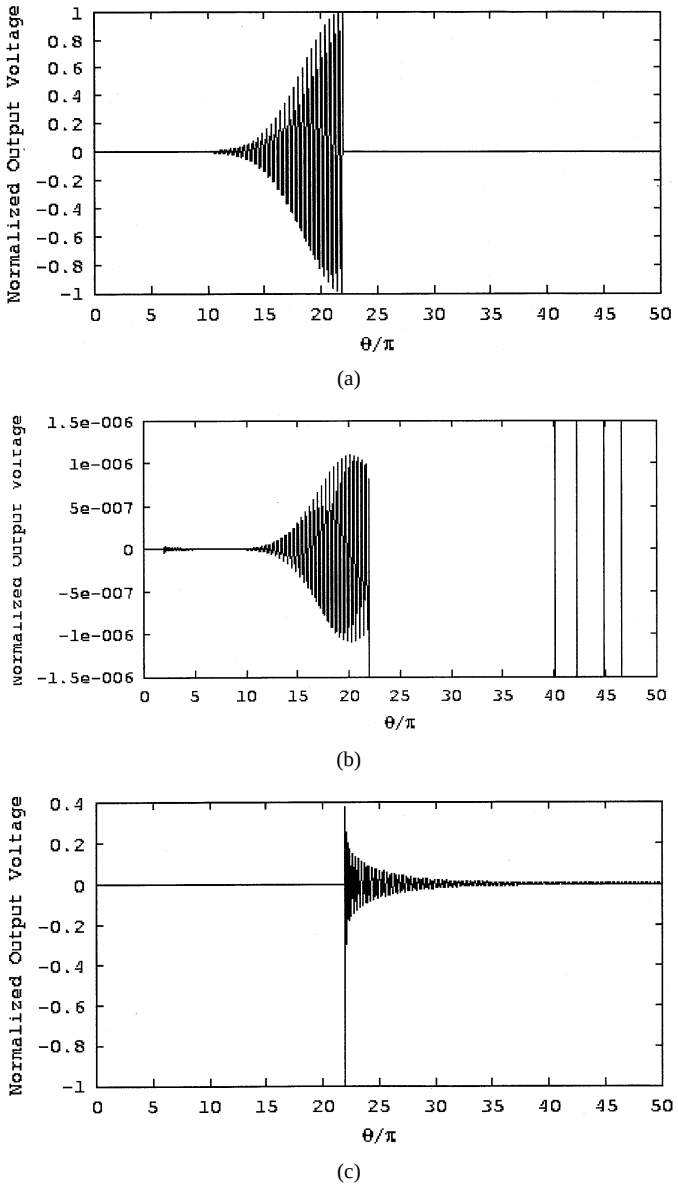

Fig. 8. TEM output (a) zoomed waveguide output and (b) non-zoomed waveguide output signals of case 4. Input signal is a carrier of $\omega_{\text{carrier}} = 0.91 \cdot \omega_{\text{cutoff}}$ modulated by a Gaussian pulse with $\theta_\tau = 5 \cdot \pi$ and $\theta_m = 20 \cdot \pi$, which is switched-off at its maximum.

hence retains its lower energy level up to the switch-off point. The jumping point of the output signal can then be uniquely associated with the switch-off point of the input signal.

Case 5: In order to allow for a multi-pulse excitation another baseband signal has been used in this and the subsequent case (case 6). The corresponding input signal is given by

$$v_S(\theta) = u(\theta) \cdot \left[\sin\left(\frac{\theta}{10}\right)\right]^4 \cdot \cos\left(\frac{\omega_{\text{carrier}}}{\omega_0} \cdot \theta\right). \qquad (20)$$

Again, $\theta_o = 2 \cdot \pi$, $\omega_{\text{carrier}} = 5 \cdot \omega_o$, $\omega_{\text{cutoff}} = 5.5 \cdot \omega_o = 1.1 \cdot \omega_{\text{carrier}}$. The input has been switched-off at $\theta = 40 \cdot \pi$, which corresponds to a four-pulse excitation. Fig. 9(a) and (b) shows the TEM and the waveguide outputs, respectively. A very interesting characteristic of evanescent transmissions is that the

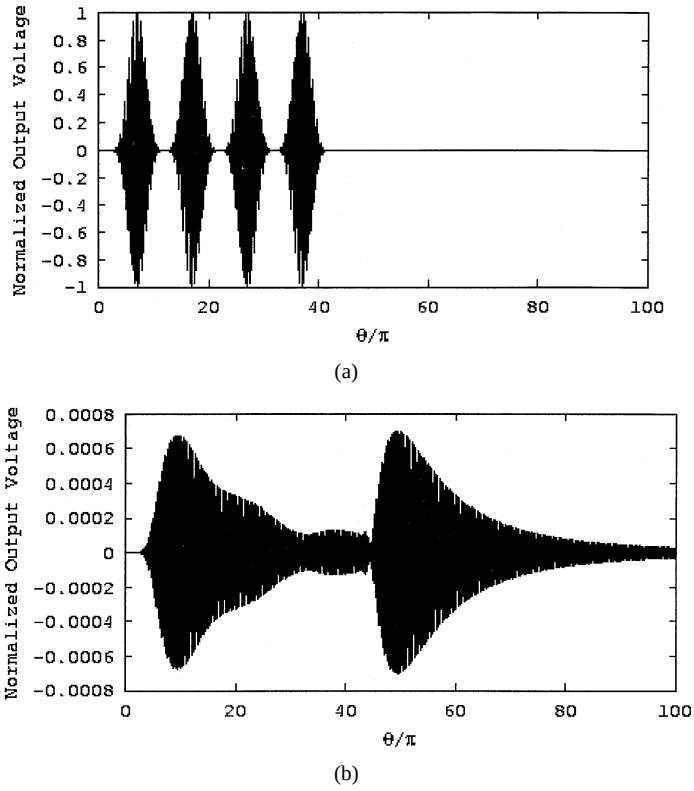

Fig. 9. TEM output (a) waveguide output and (b) signals of case 5. Input signal is a carrier of $\omega_{\text{carrier}} = 0.91 \cdot \omega_{\text{cutoff}}$ modulated by four successive pulses of a total temporal extension of $40 \cdot \pi$.

shape of the waveguide output for a multipulse excitation is not dependent on the number of input pulses. As can be easily seen from Fig. 9, the waveguide output has only two peaks. The first corresponds to the switch-on of the input signal and the second corresponds to the switch-off of the input signal. The general shape of the waveguide-output signal between these two peaks does not depend on the number of the exciting pulses. This means that waveguides operating below cutoff cannot be used to transfer high-bit-rate ***information***. In other words, in order to be able to distinguish between individual pulses (bits), one has to wait until the switch-off effect of a pulse disappears before the next pulse can be switched-on. This time spacing between information bits is extremely long in case of evanescent transmissions. This is another objection to [1] and [2] in which it has been claimed that information can be carried over evanescent modes.

Case 6: In order to complete this discussion, we considered in Fig. 10 propagation above cutoff. Here $\theta_o = 2 \cdot \pi$, $\omega_{\text{carrier}} = 5 \cdot \omega_o$ and $\omega_{\text{cutoff}} = 4 \cdot \omega_o = 0.8 \cdot \omega_{\text{carrier}}$. As in the previous case, the input signal is given by (20) with a switch-off at $\theta = 40 \cdot \pi$. It is easily seen that the waveguide output now resembles the same shape of the input signal.

It is worth noting that in all cases considered earlier the output signals for both the TEM line [Figs. 5(a)–10(a)] and the waveguide [Figs. 5(b)–10(b) as well as Figs. 6(c) and 8(c)] obey the causality and are identically zero for $\theta < \theta_o (t < L/c)$.

Cases Considered in [1] and [2]: In [1] and [2], a carrier modulated by Gaussian baseband pulses as given by (19) has been used as an input signal. The available data lead to $\theta_0 =$

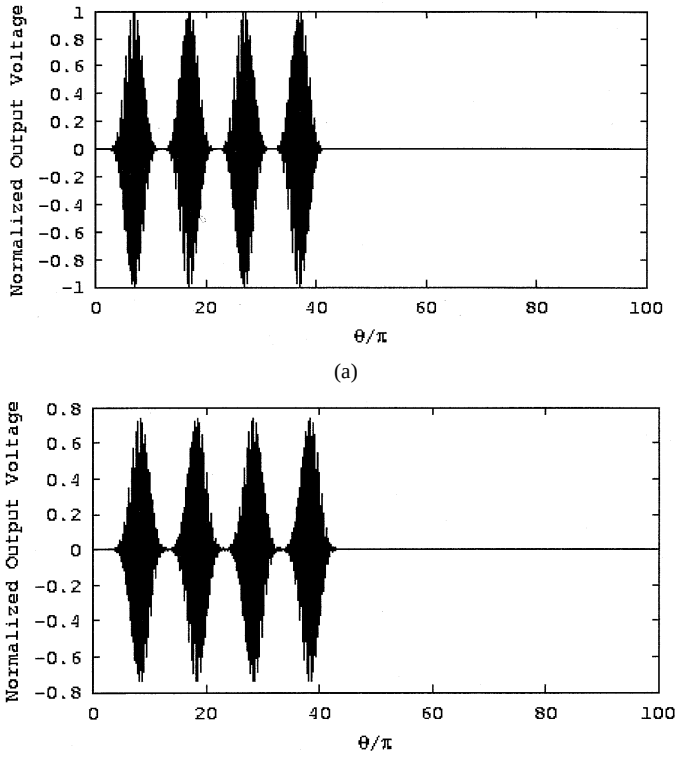

Fig. 10. TEM output (a) waveguide output and (b) signals of case 6. Input signal is a carrier of $\omega_{\text{carrier}} = 1.25 \cdot \omega_{\text{cutoff}}$ modulated by four successive pulses of a total temporal extension of $40 \cdot \pi$.

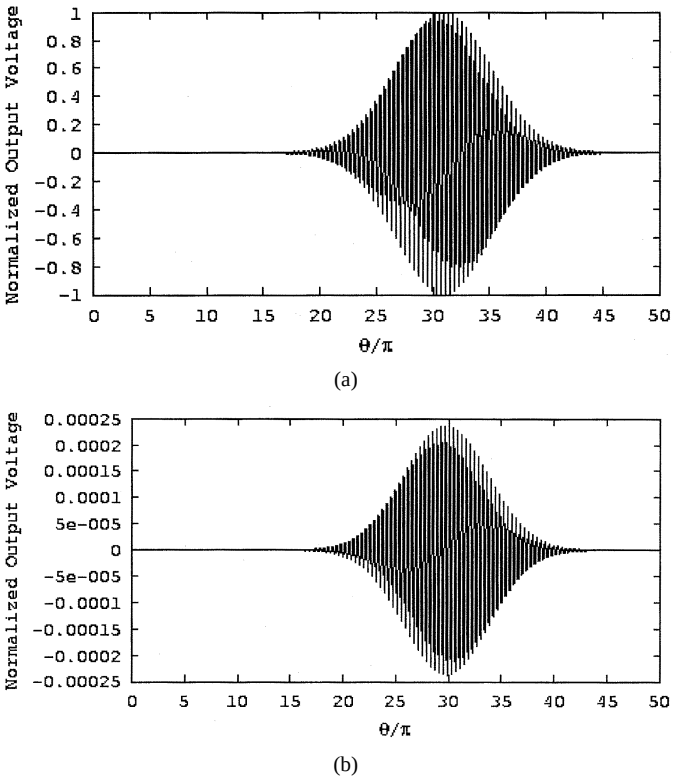

Fig. 11. TEM output (a) and waveguide output (b) signals of the case considered in [1] and [2] (modulating pulse is not switched off).

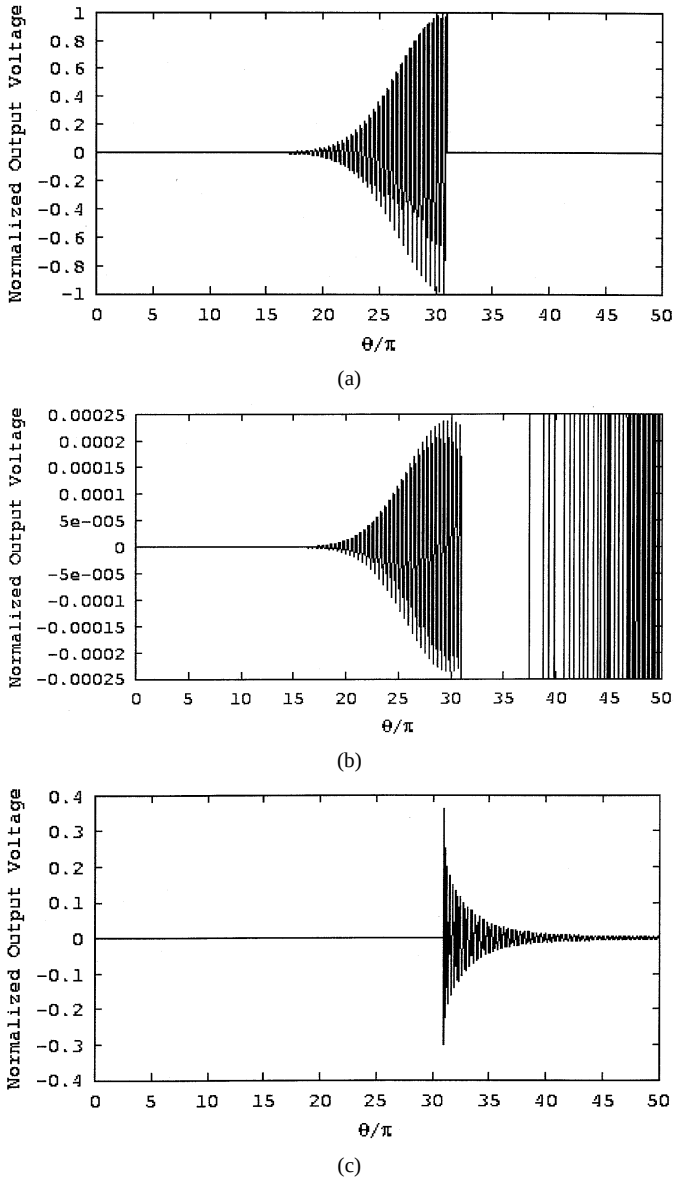

Fig. 12. TEM output (a) zoomed waveguide output (b) non-soomed waveguide output signals of the case considered in [1] and [2] (modulating pulse is switched-off at its maximum).

$1.325 \cdot \pi$, $\theta_\tau = 5.92 \cdot \pi$, and $\omega_{\text{cutoff}} = 1.0776 \cdot \omega_{\text{carrier}}$. No information about θ_m (temporal spacing between switch-on point and pulse maximum) has been available. We adopted $\theta_m = 5 \cdot \theta_\tau$ for detailed considerations. Fig. 11 represents the full pulse excitation (no switch-off), while Fig. 12 represents the corresponding half-pulse excitation (switch-off at pulse maximum). Conclusions similar to those related to Figs. 5–8 can be drawn here. Specially important is the appearance of the peak in Fig. 11(b) (at about $\theta_1 = 29.875 \cdot \pi$) earlier than the maximum of the TEM-line output in Fig. 11(a) (at $\theta_2 = 30.925 \cdot \pi$), which seems to be the reason for the incorrect assertion of the faster-than-$\boldsymbol{c}$ transmission reported in [1] and [2]. As has been stated before, such a peak has nothing to do with the maximum of the input signal. It is not more than an integration effect [see (18)] of the leading part of the input signal $v_S(\phi)$ in the range $0 \leq \phi < \theta_3 (\theta_3 = \theta_1 - \theta_0 = 28.55 \cdot \pi$, which is less than $\theta_m = 29.60 \cdot \pi$). According to the association rule we introduced before, the input maximum at θ_m is associated with $\theta_2 = 30.925 \cdot \pi$ in both the TEM-line output and waveguide

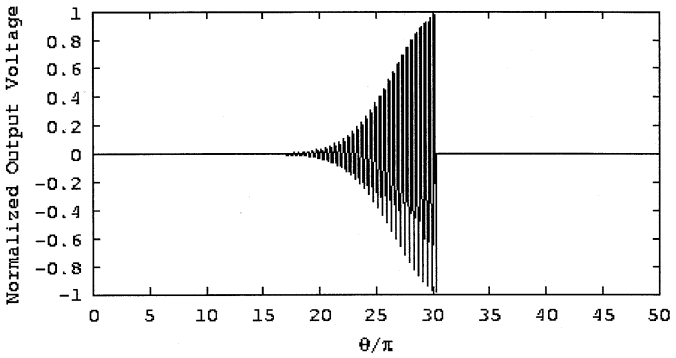

(a)

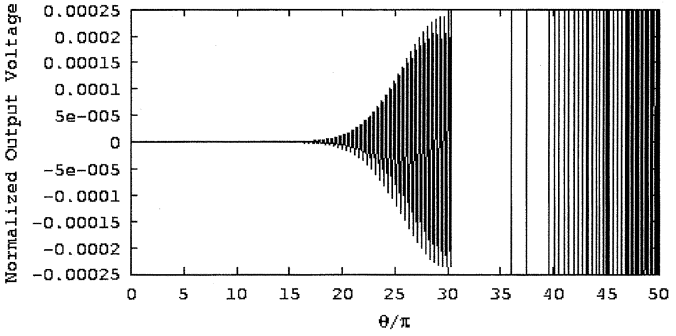

(b)

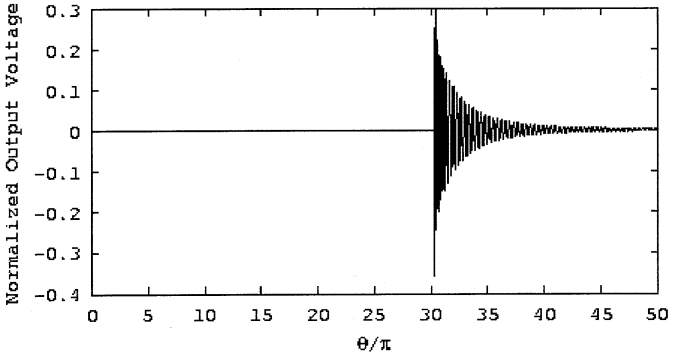

(c)

Fig. 13. TEM output (a) zoomed waveguide output (b) non-zoomed waveguide output signals of the case considered in [1] and [2] (modulating pulse is switched of before reaching its maximum).

one as may be easily seen from Fig. 12. In order to give another justification to our explanation we switched-off the input signal at $\theta = 29.00 \cdot \pi$, a value between θ_3 and θ_m. The corresponding results are shown in Fig. 13. As is easily seen, the waveguide output in Fig. 13(b) still resembles the aforementioned peak although the input has not reached its maximum at all. This is another justification that the waveguide-output peak has nothing to do with the input maximum.

IV. Conclusion

Network theoretical transient analysis of signal transmission over waveguide evanescent modes has been presented. The transfer function and the corresponding impulse response of a waveguide section with different source and load matching conditions have been revisited. Transmission of a carrier signal modulated by baseband pulses of different forms has been considered in details. It has been shown that the assertion of measurable faster-than-c signal transmission reported recently is incorrect and based on false interpretations of the measurements. Finally, evanescent mode signal transmission has been shown not to be suitable for carrying high-bit-rate information.

References

[1] G. Nimtz, "Schneller als das Licht?," Physik in unserer Zeit, 28. Jahrg., 1997.
[2] ——, "Superluminal signal velocity," *Ann. Phys. (Leipzig)*, vol. 7, pp. 618–624, 1998.
[3] L. Brillouin, *Wave Propagation and Group Velocity*. New York: Academic, 1960.
[4] J. D. Jackson, *Classical Electromagnetics*. New York: Wiley, 1975.
[5] S. Chu and S. Wong, "Linear pulse propagation in an absorbing medium," *Phys. Rev. Lett.*, vol. 48, pp. 738–741, 1982.
[6] C. G. B. Garrett and D. E. McCumber, "Propagation of a Gaussian light pulse through an anomalous dispersion medium," *Phys. Rev. Lett. A*, vol. 1, pp. 305–313, 1970.
[7] A. Pablo, L. Barbero, H. E. Hernandez-Figueroa, and E. Recami, "Propagation speed of evanescent modes," *Phys. Rev. E*, vol. 62, pp. 9628–8635, 2000.
[8] L. J. Wang, A. Kuzmich, and A. Dogariu, "Gain-assisted superluminal light propagation," *Nature*, vol. 406, pp. 277–279, 2000.
[9] X.-J. Zhou, "Possibility of a light pulse with speed greater than c," *Phys. Lett. A*, vol. 278, pp. 1–5, 2000.
[10] A. M. Shaarawi and I. M. Besieris, "Superluminal tunneling of an electromagnetic X wave through a planar slab," *Phys. Rev. E*, vol. 62, pp. 7415–7422, 2000.
[11] A. Dogariu, A. Kuzmich, H. Cao, and L. J. Wang, "Superluminal light pulse propagation via rephasing in a transparent anomalously dispersive medium," *Opt. Express*, vol. 8, pp. 344–350, 2001.
[12] R. E. Collin, *Field Theory of Guided Waves*. New York: IEEE Press, 1991.
[13] ——, *Antennas and Radiowave Propagation*. New York: McGraw-Hill, 1985.
[14] M. Abramowitz and I. A. Stegun, *Handbook of Mathematical Functions*. New York: Dover, 1972, p. 1027.
[15] A. H. Kamel and A. S. Omar, "Frequency- and time-domain expressions for transfer functions and impulse responses related to waveguide propagatio," submitted.

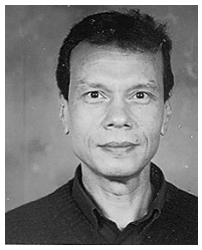

Abbas S. Omar received the B.Sc. and M.Sc. degrees from Ain Shams University, Cairo, Egypt, and the Doktor-Ing. degree from the Technical University of Hamburg-Harburg, Hamburg, Germany, all in electrical engineering in 1978, 1982, and 1986, respectively.

He has been a Professor of electrical engineering since 1990 and Head of the Department of Microwave and Communication Engineering at the University of Magdeburg, Germany, since 1998. He authored and coauthored more than 140 technical papers extending over a wide spectrum of research areas. Recently, he directed his research activities to the solution of inverse problems related to remote sensing and microwave tomography. His current research fields cover the areas of remote sensing and microwave imaging, high-speed multimedia satellite and mobile communication, electromagnetic bullets and their applications to secure, low-power, wide-band communications and subsurface tomography, stochastical electromagnetics and their meteorological, environmental, and biomedical applications, field theoretical modeling of microwave systems and components, microwave measurements and submillimeter-wave signal generation and processing.

Dr. Omar is a member of the Technical Program Committee of the IEEE MTT-S Symposium and a member of the Editorial Board of the IEEE Transactions on Microwave Theory and Techniques, IEEE Transactions on Antennas and Propagation, IEEE Transactions on Medical Imaging, IEEE *Microwave and Wireless Components Letters*, *Proceedings IEE*, *Electronics Letters*, The *Journal of Electromagnetics*, The *Canadian Journal of Physics*, and *Radio Science*.

Aladin H. Kamel received the B.Sc. and M.Sc. degrees in electrical engineering and applied mathematics, from Ain Shams University, Cairo, Egypt, in 1975 and 1978, respectively, and the Ph.D. degree in electrical engineering, from the Polytechnic University, Brooklyn, New York, in 1981.

He joined the Electrical Engineering Department of the Polytechnic University, as an Assistant Professor from 1981 to1983, the Scientific Center of IBM in Kuwait from 1983 to 1987, and the IBM Bergen Scientific Center in Norway from 1987 to 1994. Since 1994, he has been with the Regional Information Technology and Software Engineering Center, Cairo, Egypt, where he is currently the Executive Director of the center. His research areas include the mathematical and numerical modeling of wave processes (electromagnetic, acoustic, and seismic), mathematical and numerical methods for subsurface imaging using acoustic and electromagnetic reflection data, the use of advanced workstations in scientific computing and in 3-D visualization of numerical simulation results and digital image processing of satellite images and heterogeneous distributed databases. He has authored and coauthored more than 80 technical papers and reports.